(Preprint) AAS 10-140

# ICESAT ATTITUDE AND POINTING CORRECTION USING THE LASER REFERENCE SENSOR

**Sungkoo Bae,[*] Noah Smith,[†] and Bob Schutz[‡]**

The Laser Reference Sensor (LRS) is a customized commercial star tracker providing reference information for ICESat precision attitude and pointing determination. Instead of measuring multiple stars in a large field of view, it makes high angular resolution measurements of the altimeter laser beam, stars, and a reference source. The LRS has been used to correct several systematic pointing errors on the scale of 20 arcseconds down to a few arcseconds. This paper describes significant LRS results and possibilities for future reference instruments.

## INTRODUCTION

The Ice, Cloud, and land Elevation Satellite (ICESat) was launched on January 12, 2003. The science instrument is the Geoscience Laser Altimeter System (GLAS), designed and built at Goddard Space Flight Center. The primary objective is to make ice sheet elevation measurements in the polar region in order to determine the mass balance of the ice sheets and their contributions to global sea level change.[1] Laser pulse time of travel is used to compute the distance between GLAS and laser spot positions. Precision Attitude Determination (PAD) and Precision Pointing Determination (PPD) estimate the direction of the laser pulse as a unit vector in the GLAS and inertial coordinate frames. The position vector of GLAS in inertial space is estimated by Precision Orbit Determination. The position and surface elevation of laser spots are determined by combining the laser pointing direction, GLAS position vector, and laser travel distance.

GLAS performs narrow beam laser altimetry with one of three identical Nd:YAG laser sources operating at a 40 Hz pulse repetition rate and wavelength of 1064 nm. It also measures atmospheric backscatter profiles at both 1064 and 532 nm for atmosphere science. The 532 nm signal is produced by frequency-doubling the 1064 nm output of the lasers.[2] The lasers, pulse optical path, telescope and other instrumentation are mounted on a stable optical bench. Thermal control is provided by a system of heat pipes and radiators.

Accurate attitude and pointing estimation is needed to meet the GLAS science requirements, which are defined by an error budget and ancillary information.[3] The PPD requirement is that laser spot positions on the ground be known to within 7.5 cm ($1\sigma$), which is equivalent to 1.5 arcseconds for the 600 km orbit and a 1° slope of the surface. Several GLAS instruments are de-

[*] Research Associate, Center for Space Research, The University of Texas, Austin, TX 78712
[†] Graduate Student, Center for Space Research, The University of Texas, Austin, TX 78712
[‡] Professor and Associate Director for Center for Space Research, The University of Texas, Austin, TX 78712

signed for pointing determination. They are described in the next section. The Laser Reference Sensor (LRS) is one of these instruments, and is the central topic of this paper. It is a unique instrument designed specifically for ICESat PPD. An improved LRS-2 design for the ICESat-II mission is also discussed.

## GLAS LASER POINTING DETERMINATION

The Stellar Reference System (SRS) was designed to measure the inertial direction of GLAS laser pulses to within 1.5 arcseconds at 10 Hz. A conceptual sketch of the SRS is shown in Figure 1. To reduce alignment variations, all of the SRS components are attached to the GLAS optical bench. The primary sensors are: Instrument Star Tracker (IST), Laser Reference Sensor (LRS), Laser Profiling Array (LPA), and Space Inertial Reference Unit (SIRU) containing four Hemispherical Resonator Gyros. The LPA measures the intensity profile of the laser beam at 40 Hz. Originally the LRS was designed to operate at 40 Hz to measure all of the 40 Hz laser pulses. The LRS rate was reduced to 10 Hz and the 40 Hz LPA was introduced. The LRS measures one out of the four pulses measured by the LPA, not an average of the four pulses.

Pointing determination begins with attitude estimation using data from the IST and SIRU. The IST is an unmodified Goodrich HD-1003 CCD star tracker. It observes up to 6 stars simultaneously in an 8°×8° field of view at 10 Hz. Attitude estimation provides the IST orientation relative to the celestial reference frame.

A fraction of the laser beam is redirected into the LRS. It views both the sky and the beam simultaneously. In effect it projects the beam backwards onto the sky. An HD-1003 star tracker was modified to act as the LRS detector. The LRS field of view is 0.5°×0.5° instead of 8°×8°, and the 10 Hz sampling rate captures one out of four laser pulses. Some bright stars are measured simultaneously by both the LRS and IST. These shared stars provide a reference link between the laser beam, the IST attitude estimate, and the sky.

An additional instrument, the Collimated Reference Source (CRS), also ties the LRS to the IST. It is mounted on the IST and transmits a laser beam which is redirected into the LRS. The CRS uses a fraction of the 532 nm laser pulse. The dependence of the CRS on the 532 nm portion of the primary laser beam was a major issue for pointing determination.

Two Ball CT-602 star trackers (BST1 and BST2) are mounted on the spacecraft bus for real-time attitude determination and control. They are pointed 30° to either side of the IST optical axis. Each BST has an 8°×8° field of view and observes up to 5 stars at 10 Hz. BST performance is at least as good as IST performance, but the BSTs are not optimal for laser pointing determination. A star tracker attitude estimate is less certain about the optical axis because of the small field of view. This is not an issue for the IST because its optical axis is parallel to the laser beam. The BST optical axes are not parallel to the laser beam, which increases uncertainties for laser pointing determination. BST attitude estimates have however been useful for finding unexpected issues in the IST attitude estimates.

## LASER CAMPAIGNS

The mission plan was to use the three identical laser sources sequentially for continuous science operation throughout a three to five year mission. The flight history is more complex because of a problem in the laser source design. Laser 1 was activated five weeks after launch and

failed after 38 days of useful data. A GSFC review board determined that the cause was in the design and common to all three lasers.

For the two remaining lasers, a modified plan was created. The lasers were operated two or three times per year for periods of about thirty days called campaigns. Spring, summer and fall campaigns were performed until 2007, spring and fall campaigns after 2007. Laser 2 was activated in September 2003. Its output energy decayed rapidly, but techniques for slowing the decay were developed. Laser 3 was used from October 2004 to October 2008. The remaining capability of Laser 2 was used from November 2008 to October 2009. Individual laser campaigns are named by combining a laser number and an alphabetic character representing chronological order. For example Laser 2a is the first campaign with Laser 2 and Laser 2b is the second. Here calendar dates are often also given.

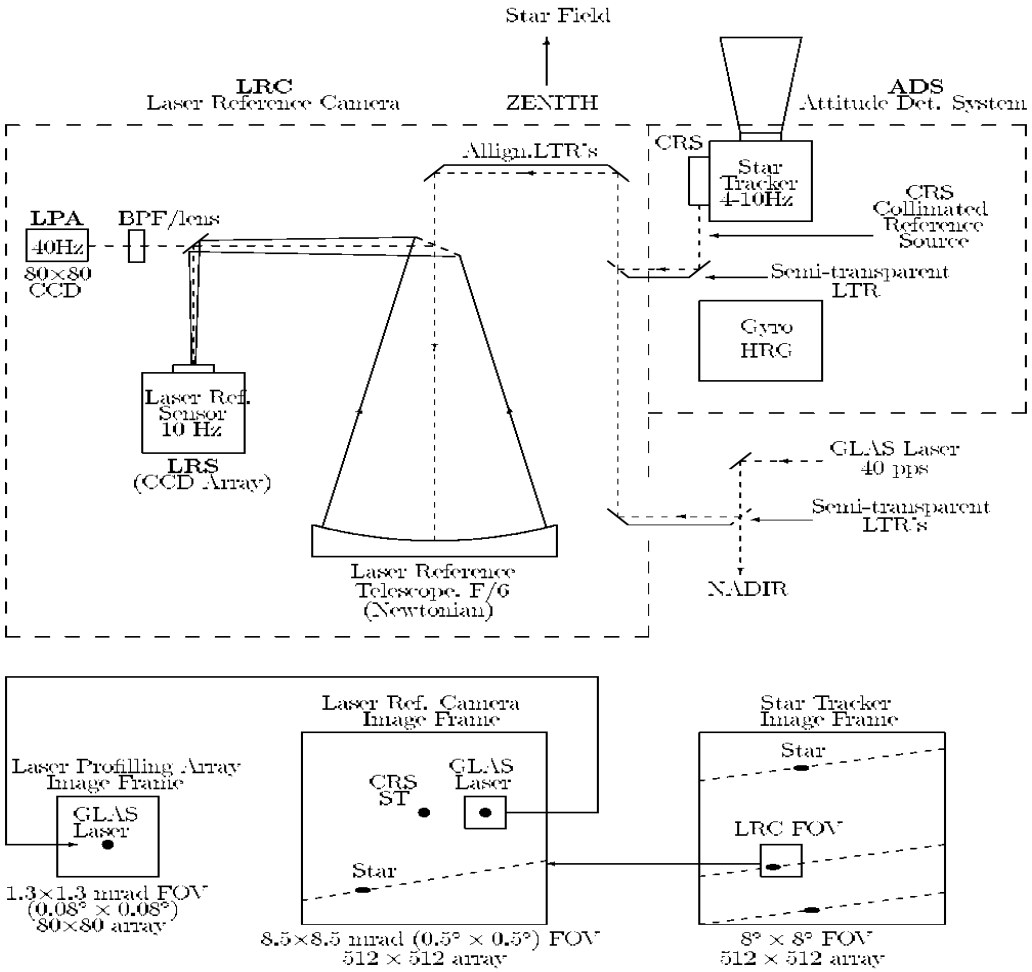


**Figure 1. Stellar Reference System**

## ATTITUDE MODES

Two attitude modes are used depending on the angle between the sun and orbit plane: sailboat mode, and airplane mode. They are designed to maximize illumination of the solar panels while minimizing the number of yaw maneuvers. In sailboat mode the spacecraft velocity vector is parallel to the solar panel rotation axis. In airplane mode the velocity vector is perpendicular to the solar panel rotation axis. Within each mode there are two sub-modes 180° apart. In sailboat mode, one or the other sub-mode is used continuously until the switch to airplane mode near the sun. The yaw maneuvers to change modes are performed regularly and do not directly affect processing. Airplane mode does however have some special characteristics, primarily due to sun blinding of the star trackers.

Airplane mode is used when the sun is within 33° of the orbit plane. During airplane mode the sun approaches, passes through, and departs from the orbit plane. When it passes through the plane the airplane sub-mode is changed by a 180° yaw maneuver. The IST optical axis is also in the orbit plane. When the sun passes through the orbit plane it is also passing directly through the IST field of view once per revolution. The result is IST data gaps due to sun blinding, once per revolution growing as the sun approaches the plane and then shrinking as the sun departs the plane. The maximum data gap is about 800 seconds or 14% of an orbital revolution.

## PAD AND PPD IMPLEMENTATION

The algorithm developed for the SRS system was implemented as PAD and PPD ground processing software.[4] The PAD software estimates the attitude of the IST frame using IST and SIRU data. The PPD software estimates the direction of the laser with respect to the IST and celestial frames using IST, LRS and LPA data.

The LRS frame is tied directly to the IST frame by the star measurements since the LRS star should be found in the star field covered by IST field of view. Alignment parameters between the LRS and IST frames are estimated using the LRS star measurements. The alignment determines the IST frame position of the laser spot measured by the LRS.

The LRS ties the LPA frame to the IST frame. One out of four 40 Hz laser pulses is measured simultaneously by both the LRS and the LPA. Alignment parameters between the LRS and LPA are estimated using the simultaneous measurements. Together, the LPA to LRS and LRS to IST alignments determine the IST frame position of both the LPA and LRS laser spot measurements. The result is that shot to shot variations of the laser pointing vectors are estimated in the IST frame and celestial frame at 40 Hz.

The description above assumes that the instruments perform as designed. One flight issue appeared immediately. The LRS is sensitive to sunlight scattering from the edge of its sun shade. Too much scattered light reaches the detector. After activation in February 2003 it consistently reset in sunlight. It had to be disabled in sunlight, requiring considerable ground activity. After about two weeks of partial operation it was deactivated until a software patch was uploaded. Restricted LRS operation resumed with the Laser 2a campaign in fall 2003. After modification, the laser spot and CRS spot measurements are continuous, star measurements are not made in sunlight.

The periodic absence of LRS star measurements because of sunlight modified the processing software. Pre-launch measurements of the alignment of the laser beam and IST are used as reference values for determining the alignment variations. Attitude estimation using the IST and SIRU data proceeds normally. An ocean scan maneuver[5] was used to estimate corrections to the refer-

ence rotation between the IST optical axis vector and the laser pointing vector. These corrections resulted in better elevation products, and made further calibrations possible.

## LRS OBSERVATIONS

The LRS observes stars, the primary laser spot, and the CRS laser spot. The field of view is 0.5°×0.5° and the measurement rate is 10 Hz. The LRS optics is defocused to spread the images over multiple pixels. Each image is observed by a software virtual tracker. Centroiding is performed internally and the output is a measured unit vector in the LRS frame. Raw image data are transmitted to the ground for diagnostic purpose; only 10 images per second, 5 star virtual tracker images, 4 laser virtual tracker images, and 1 CRS virtual tracker image. The virtual tracker images are 16×16 pixels.

Both LRS and LPA images show the distribution of intensity in the laser beam. The beams were distinctly different for each of the three laser sources. Smaller changes for a single laser source from campaign to campaign were also clear, mostly related to the decrease of intensity with time. Images of all three laser sources are shown in Figure 2.

LRS images of Laser 1 initially had an elliptical center with an irregular shape at one edge as shown in Figure 2a. The LRS was temporarily deactivated and only LPA images of the laser were available for the remainder of Laser 1. An LPA image with rotated axes from later in Laser 1 is shown in Figure 2b. The irregular shape grew and detached from the central ellipse over about 30 days. Laser 2 laser images were elliptical like Laser 1, but without irregularities. Laser 2 images from different campaigns six months apart are shown in Figures 2c and 2d. The ellipse orientation changes but the size and shape are constant. Laser 3 laser images were roughly circular and constant over four years of operation. An early Laser 3 image is shown in Figure 2e and a late image is shown in Figure 2f.

All 40 Hz LPA laser images are transmitted to the ground. PPD processing includes computation of the image centroid, intensity, major axis, eccentricity, and orientation with the assumption that the laser images are elliptical Gaussian distributions. Information from orbit determination is used to calculate orientation as the angle from topocentric north. LPA images are compared to ground measurements of the laser profile. They were also compared with simultaneous pictures taken from an airplane over the White Sands detector array.[6] LPA laser images should be similar to LRS laser images except for a 90° rotation as shown in Figure 2b.

The LRS also observes the CRS laser beam. A CRS image observed during the Laser 1 campaign (February-March 2003) is shown in Figure 3a. When Laser 2 was activated in September 2003 the CRS image was smaller. The CRS intensity of Laser 2 was less than half of Laser 1 due to reduced energy in the 532 nm laser channel.

A typical LRS star image is shown in Figure 3b. The star images are sometimes more elliptical than circular. The difference between CRS, laser, and star measured intensities is larger than Figure 3 suggests. Measured CRS and laser intensities are tens or hundreds of times larger than measured star intensities, depending on the brightness of the star. Because of the small LRS field of view, the LRS has higher angular resolution than the IST. The spacecraft's solar array induced 1 Hz oscillations are fully resolved by the LRS star measurements as shown in Figure 4a. IST measurements of a bright star with magnitude 3.9 at the same time are noisier as shown in Figure 4b. This example of IST measurements is a best case scenario. Most IST stars are dimmer and noisier.

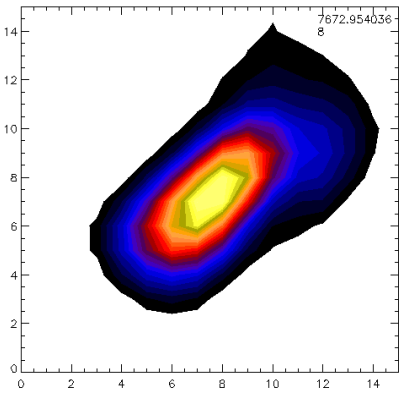


**(a) Laser 1 LRS image (058/ 2003)**

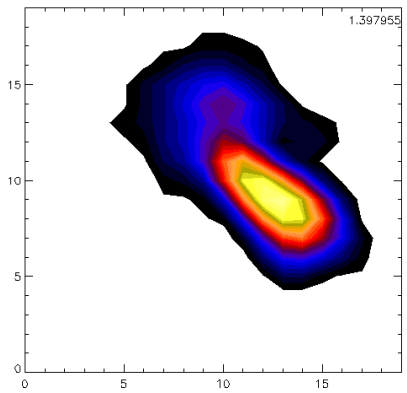


**(b) Laser 1 LPA image (065/2003)**

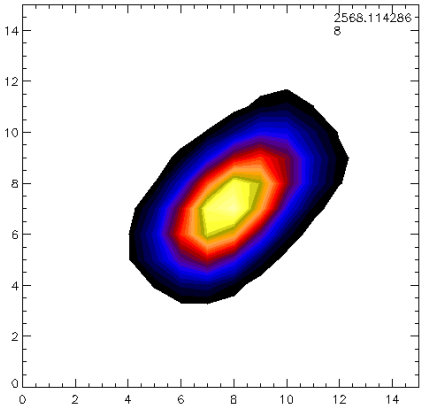


**(c) Laser 2 LRS image (269/2003)**

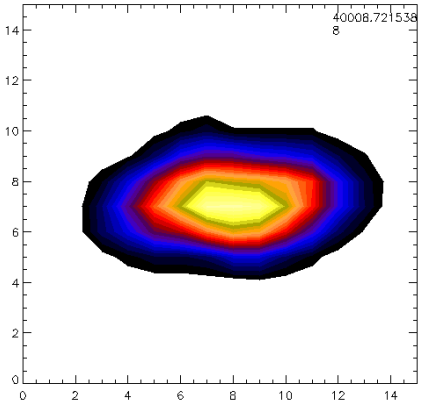


**(d) Laser 2 LRS image (146/2004)**

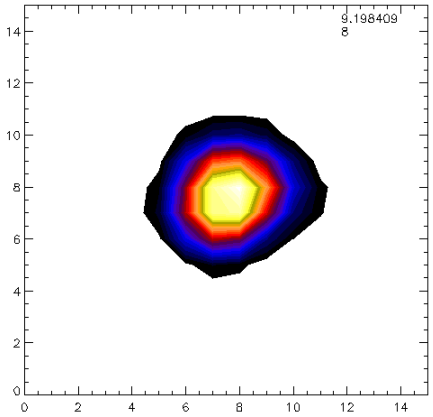


**(e) Laser 3 LRS image (278/2004)**

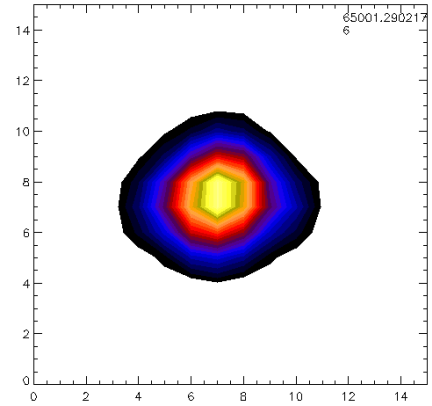


**(f) Laser 3 LRS image (279/2008)**

**Figure 2. Laser images observed by LRS or LPA (day/year)**

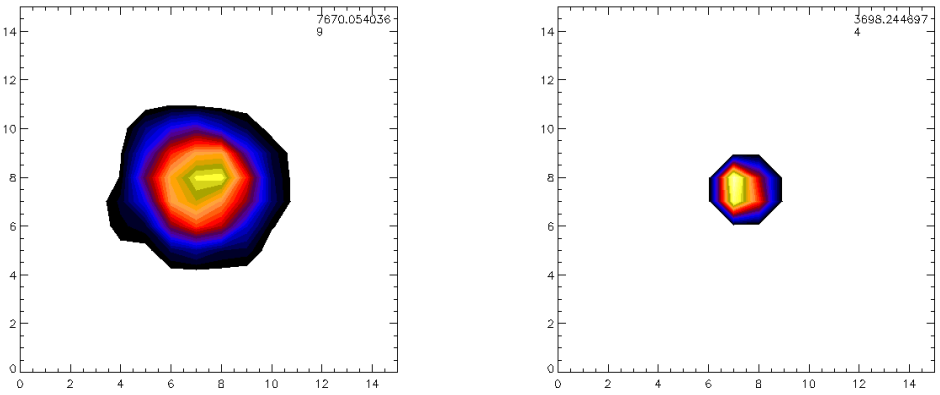


**(a) LRS CRS image (058/2003)** **(b) LRS star image (282/2007)**

**Figure 3. CRS and star image samples (day/year)**

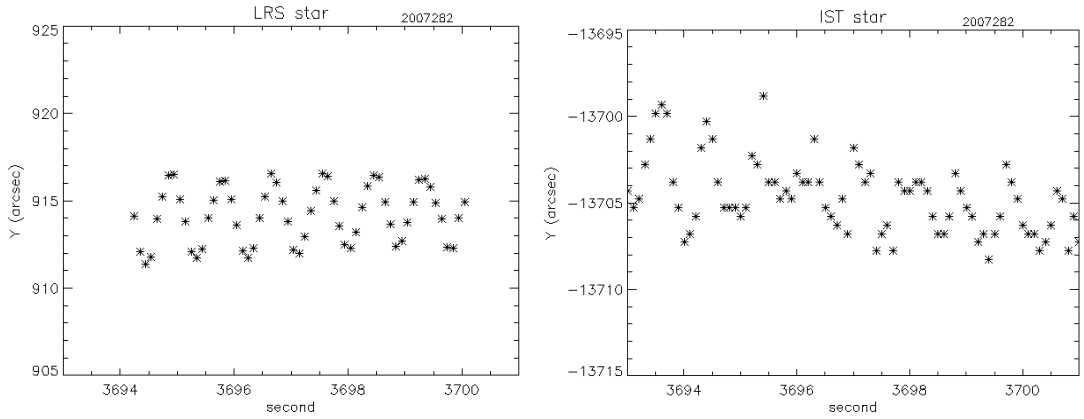


**(a) LRS star centroids (282/2007)** **(b) IST star centroids (282/2007)**

**Figure 4. Star motion observed by LRS and IST (day/year)**

## LRS OBSERVATIONS OF IST ALIGNMENT VARIATIONS

The limited LRS data during Laser 1 showed periodic motion of the CRS spot. The CRS is rigidly attached to the IST. The motion correlated with orbital position and was caused by motion of the IST relative to the LRS. The magnitude and character of the CRS spot motion agreed with a separate result from ocean scan calibrations. As mentioned, an ocean scan maneuver was developed to estimate corrections to the reference rotation between the IST optical axis vector and the laser pointing vector. If the relative motion between the IST and LRS is not included in the ocean scan corrections, the laser pointing results show a residual variation. The variation has a peak-to-peak magnitude of 20 arcseconds and correlates with the sunlit and shadowed portions of the orbit.

CRS spot positions were observed continuously during Laser 2a (September-November 2003). Orbital variations over one day (day 274) are shown in Figure 5a. They are almost identical from orbit to orbit. They change over days with the relative position of the sun, but the change is usually too small to notice within a day. Variations over one orbital period, starting from orbit midnight*, are shown in Figure 5b.

Near orbit midnight the CRS spot position was roughly constant. ICESat was on the opposite side of the earth from the sun, and the optical bench and IST alignment were thermally stable. Near 90° orbit angle sunlight began to hit the IST and its temperature increased rapidly. The IST alignment also changed rapidly, as shown by the variation of the CRS spot position around 2600 seconds in Figure 5b. Near 270° orbit angle sunlight left the IST and the CRS spot position slowly decayed.

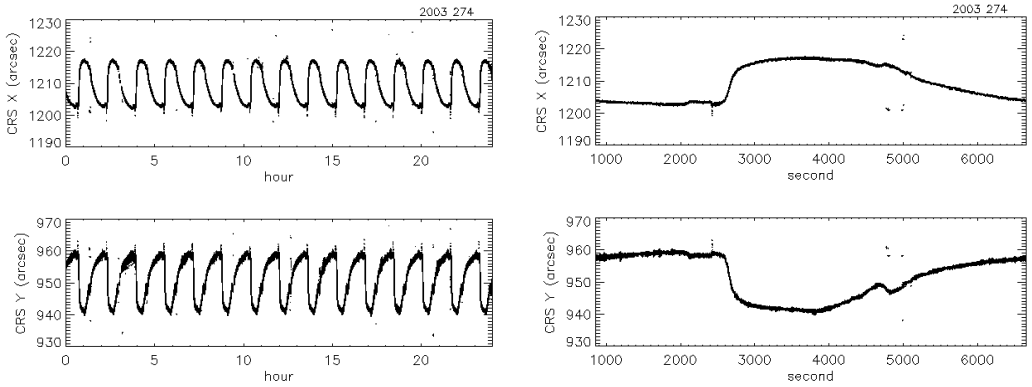


**(a) CRS orbital variation for a day** **(b) CRS orbital variation for one revolution**

**Figure 5. LRS measurements of CRS spot position in early Laser 2a (day 274 of year 2003)**

The CRS signal weakened along with the 532 nm laser intensity during Laser 2a. LRS measurements of the CRS spot positions became noisier. Noise first appeared at the beginning of the rapid change of the position curves, near 90° orbit angle. This change is clear at around 2100 seconds in Figure 6a. The cause is thought to be a combination of light scattering from the IST sunshade and the weak 532 nm laser intensity. The noise grew more widespread throughout the orbit, and significant data gaps appeared around 90° and 270°, as shown in Figure 6b.

CRS data was used to correct IST alignment variations during Laser 2a, despite the decreasing CRS quality. Corrections were applied to the IST unit vector measurements. Pointing determination results showed significant improvements based on comparisons with scan maneuvers, White Sands observations, and crossover analysis.[7]

CRS data became too noisy for correcting IST alignment during Laser 2b (February-March 2004). The CRS spot was no longer available by the middle of Laser 2c (May-June 2004). The CRS was replaced by a batch-EKF correction method[8] before Laser 3a (October-November 2004). The batch-EKF correction estimates IST alignment corrections using IST and SIRU data. Performance of the new method was verified by comparing it with the CRS data from Laser 2a. The batch-EKF corrections have the same characteristics as the CRS corrections.

* Orbit midnight is defined as when the angle between the IST boresight vector and the sun vector is at its maximum. In this paper, orbit angle is defined as 0° at orbit midnight, 90°/270° in the polar regions, and 180° at orbit noon.

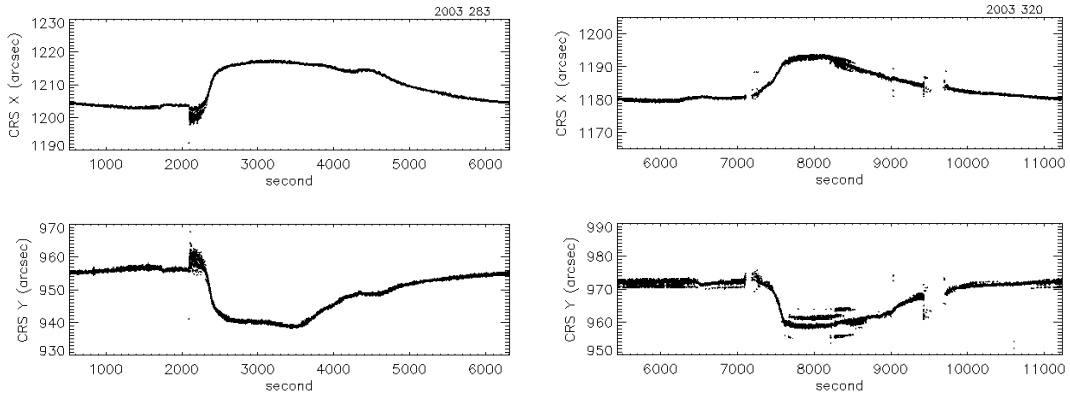


**(a) CRS orbital variation on day 283** **(b) CRS orbital variation on day 320**

**Figure 6. CRS data observed by LRS in middle and end of Laser 2a campaign in 2003**

## LRS OBSERVATIONS FOR LASER MOTION CORRECTION

Laser spot positions in the LRS also had orbital variations. The size of the laser variation was much smaller than the CRS variation, but large enough to indicate that the alignment of the laser source and LRS varied. Laser spot positions in the LPA showed nearly identical variations. The similarity of position, size, and shape of laser images in the LRS and LPA indicated there was little alignment variation between them, as shown in Figure 7.

When CRS data was available early in the mission, corrections for both the CRS and laser variations were applied simultaneously to the IST star measurements. After the batch-EKF method replaced the CRS, laser motion was corrected separately from IST alignment correction. LRS data was not available at various times, for example after the LRS shutdown in Laser 1 and for two days during Laser 3f (May-June 2006). LPA data was used for laser motion corrections at these times.

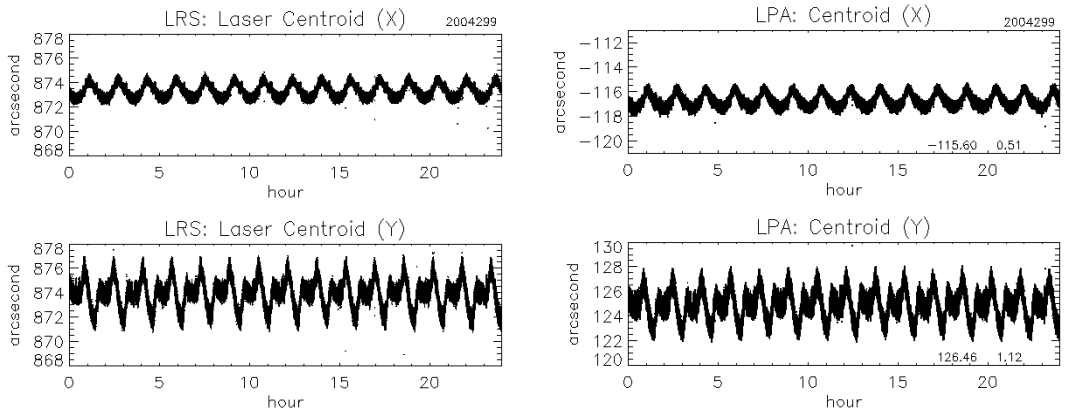


**(a) LRS laser motion** **(b) LPA laser motion**

**Figure 7. Laser motion observed by LRS and LPA (day 299 of year 2004)**

## LRS CORRECTION OF IST TIME-TAG JUMPS

The angles between the IST boresight and each of the BST boresights were nominally 30°. These angles varied periodically due to relative motions of the star trackers. The angles between boresights also had slow non-periodic variations, correlated with changes of the sun's position relative to the ICESat orbit plane. In addition, GLAS may have moved with respect to the spacecraft bus. Plots of angular variations between the boresight directions were used to monitor these motions and validate PAD results.

Jumps of about 22 arcseconds were observed in the angles between the IST and BST1 boresights in Laser 2a, as shown in Figure 8a. Similar jumps were also observed between the IST and BST2, with reversed direction. Laser 2a was in sailboat mode with the three boresight vectors in a plane perpendicular to the spacecraft angular rate vector. The jump size of 22 arcseconds suggested time-tag errors. The spacecraft rotates at 223 arcseconds per second and the trackers operate at 10 Hz. An error of 0.1 seconds in one of the tracker time-tags would result in 22 arcseconds of alignment error in the plane of the boresight vectors.

The jumps were not fully investigated until issues arose in the elevation products of Laser 3c (May-June 2005). Ground elevations based on normal PAD processing showed anomalies when compared to ocean data results.[9] Daily mean values* for 15 out of the 33 days were not in the expected range. Initially, the angles between the boresights appeared normal for all 33 days, but a three axis analysis revealed jumps that were concealed by the attitude mode. Laser 3c was in airplane mode with the three boresight vectors and the spacecraft angular rate vector all in the same plane. A tracker time-tag error would not affect the boresight angles. Instead, rotations between the three dimensional tracker quaternions showed jump discontinuities, as shown in Figure 8b. The jumps were found on the anomalous days and there was a correlation between the number of jumps and the size of the ocean data anomaly.

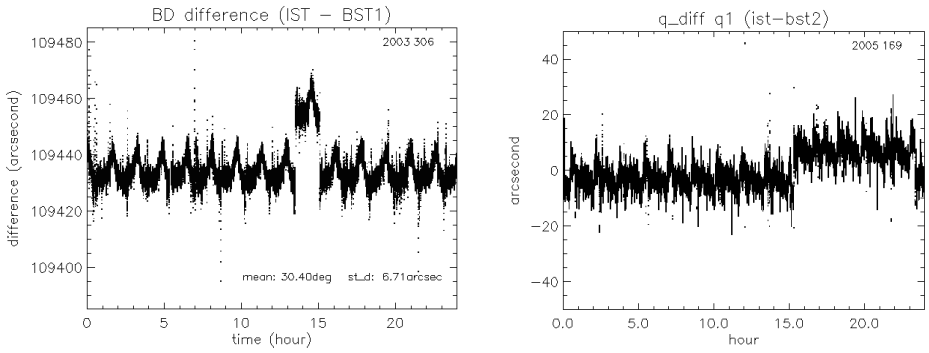


**(a) boresight difference (306/2003)** **(b) quaternion difference (169/2005)**

**Figure 8. attitude solution differences between IST and BST using boresights(a) and a quaternion component(b)**

* Ocean data analysis is a method for validation of the ICESat elevation products. ICESat elevations over the ocean are compared to elevations from mean sea surface. One of the parameters regularly compared is the daily mean of the elevation difference.

The Laser 3c jumps always began and ended during IST sun-blinding when no IST star data was available. IST data gaps due to moon-blinding were present at the beginning and end of jumps during sailboat mode. In Figure 8a, moon-blinding caused 200 second IST data gaps at the first and second jumps. Jumps occurred with IST blinding data gaps, and were much more frequent in airplane-mode because of sun-blinding. This was confirmed by comparing attitude quaternions propagated using SIRU and IST data.

There was also a correlation between jumps and attitude sub-mode. Jumps were more frequent in the airplane sub-mode with yaw angle 0° than the sub-mode with yaw angle 180°. As mentioned, within each attitude mode there are two sub-modes 180° apart. During airplane mode the sun approaches, passes through, and departs from the orbit plane. When it passes through the plane the airplane sub-mode is changed by a 180° yaw maneuver. This suggests that the jumps are related to the direction of star motion relative to the IST.

Time-tag jumps during IST blinding data gaps could have been inherent in the raw spacecraft data, or introduced by ground processing. The question was complicated by a different type of IST time-tag issue with similar characteristics. Every day, regardless of external factors, there were approximately 15,000 0.1 second time-tag errors. These errors were found to be caused by how the IST center of integration time was handled.[10]

LRS data was used to find that the IST blinding time-tag jumps were in the raw spacecraft data. The LRS was used to examine bright stars measured simultaneously by the LRS and IST on multiple succeeding orbital revolutions. A quaternion component difference between the IST and BST1 showing the alignment jump due to an IST blinding time-tag jump is shown in Figure 9. At the marked times, the same bright star was measured by both the IST and LRS. During the time-tag jump, the IST measurements of the star had a 22 arcsecond offset relative to the LRS measurements.[10]

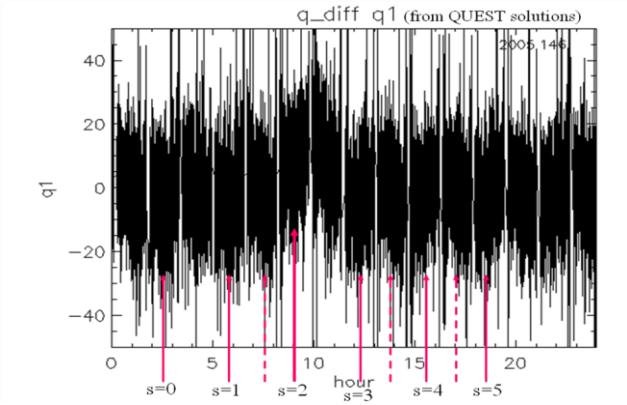


**Figure 9. A component of the attitude quaternion difference between IST and BST1 for day 146 of year 2005. Simultaneous measurements of a bright star by the LRS and IST on succeeding revolutions are indicated.**

Quaternion differences between the IST and BSTs were used to find the approximate starting and ending times of the IST blinding time-tag jumps. IST time-tags were then corrected before PAD processing. With the corrected time-tags, the quaternion differences did not contain jumps. The anomalies in Laser 3c ocean daily mean values disappeared. The root cause of the IST blinding time-tag jumps is not yet understood. When the jumps begin and end, there is no IST star data. The question is made more difficult by the other IST time-tag issue with frequent 0.1 second errors.

## LRS CORRECTION OF SIRU TIME-TAG SHIFT

There was a 2.8 Hz oscillation in elevation results over a flat Bolivian salt lake on day 293 of 2003. The 2.8 Hz signal is regularly observed in the SIRU data and believed to be a response of the spacecraft to changes of solar array position. Both 1 Hz and 2.8 Hz oscillations from the solar arrays are clear in the SIRU and LRS data. An example of the LRS 1 Hz signal is shown in Figure 4a. The oscillations are not as clear in the IST and BST data because of lower resolution as shown in Figure 4b. In the case of the Bolivian salt lake, both PAD and PPD results showed a 2.8 Hz signal. The fact that the signal propagated beyond PPD and appeared in higher-level elevation results indicated there were additional errors in the PPD results. The suspected error source was a time synchronization problem between the IST and SIRU.

LRS data was used to examine SIRU time-tags and a 50 millisecond shift was discovered. Using corrected time-tags, the 2.8 Hz oscillation in elevation results for the Bolivian salt lake disappeared. After its discovery, the 50 millisecond correction was applied in all processing. The LRS was used by comparing the motion of a star in the LRS to the angles output by the SIRU. The SIRU output was sets of three angles and time-tags. The angles were transformed to the LRS frame and then matched to the variation of the LRS star position.

After the 50 millisecond SIRU correction, there was still a small and variable time offset between the SIRU and LRS. It was monitored using LRS stars and may be additional error in the SIRU time-tags or error in the LRS time-tags. During Laser 3h (March-April 2007) the number of good LRS star was around 200 per day. SIRU time-tag offsets were computed whenever a good LRS star was available. Daily averages of the offsets for the 33 days in Laser 3h are shown in Figure 10a. The mean daily offset was -6.4 milliseconds. Campaign mean offsets from Laser 1 (February-March 2003) to Laser 3j (February-March 2008)* are shown in Figure 10b. The mean campaign offset was -6.8 milliseconds.

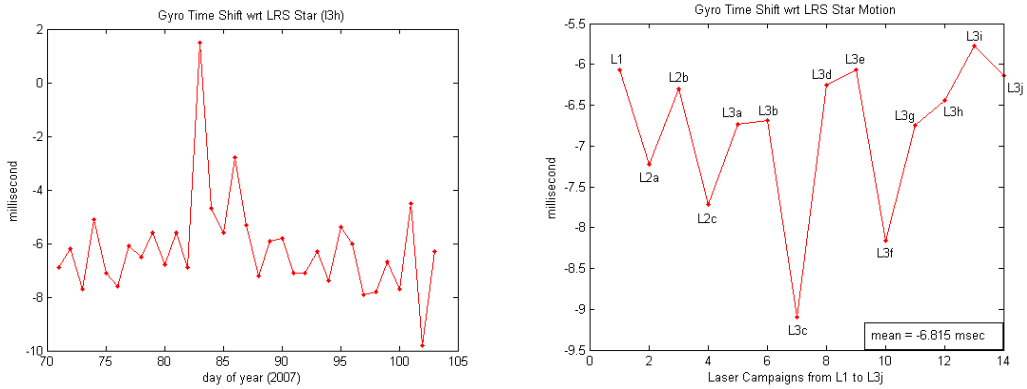


**(a) Daily averages during Laser 3h** **(b) Campaign averages until Laser 3j**

**Figure 10. SIRU time-tag offsets with respect to the LRS star motion after 50 millisecond correction of SIRU data.**

* During Laser 3j the LRS had sporadic failures. The star measurement window was disabled and only laser position measurements were made. The star measurement window was enabled from the next campaign (Laser 3k) and will be used for SIRU time-tag offsets.

## LRS OBSERVATIONS FOR EVALUATING PAD

The LRS star was also used to compare the LRS and IST time-tags. Instead of direct comparison of the IST star that was too noisy, the IST attitude estimates were converted to angular rates and integrated to give IST output with the same form as the SIRU output. The LRS and SIRU time-tag method could then be applied to the IST. Single sample QUEST[11] attitude estimates from the IST were used. Single sample attitude estimates were relatively noisy, so the derived IST motion was not as smooth as the LRS and SIRU motion. The IST motion was generally not very smooth, as shown in Figure 11a. Occasionally the star measurements were ideal and IST motion was smoother as shown in Figure 11b. The result was that no time-tag offset was found between the LRS and IST.

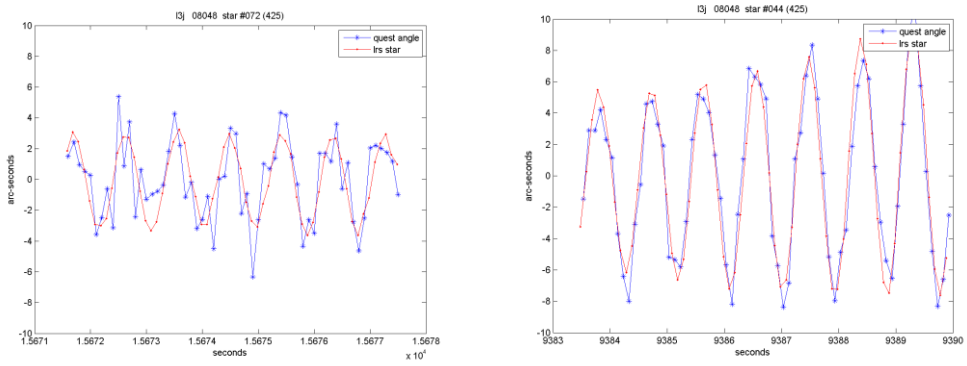


**(a) LRS star vs coarse IST motion** **(b) LRS star vs smooth IST motion**

**Figure 11. Comparison of the QUEST-derived IST motion to LRS star on day 48 of year 2008**

LRS star motion is useful for evaluating the results from the PAD extended Kalman filter using input from the IST and SIRU. The method described above for SIRU time-tag calibration is used. The attitude estimates are converted to angles and compared to the LRS star position. Angles derived from the EKF agree well with the LRS star, as shown in Figure 12. Overall, EKF results agree with the LRS star to the sub-arcsecond level. Similar results were obtained when each of BST data was used instead of IST data.

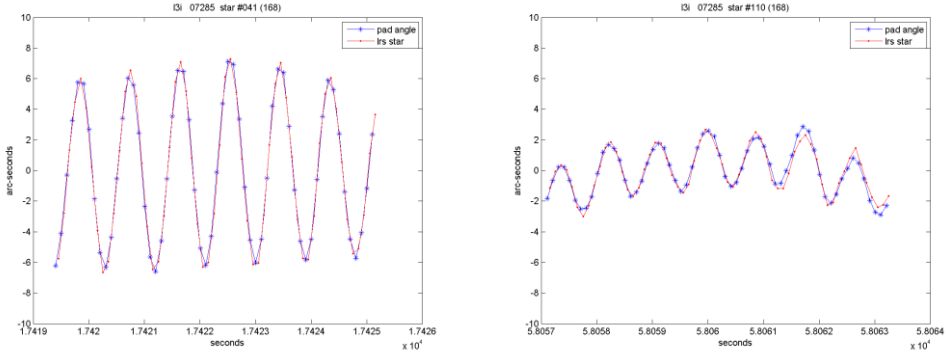


**(a) During high amplitude oscillation** **(b) During low amplitude oscillation**

**Figure 12. Comparison of the EKF-derived IST motion to LRS star motion on day 285 of year 2007. EKF-derived BST1 and BST2 motions showed similar performances.**

LRS star motion could only be used for short comparisons with the SIRU and IST because of the small LRS field of view. A typical LRS star passed through the field of view in about 7 seconds. The same type of comparison could be made between the SIRU and PAD results for longer time intervals, as shown in Figure 13. Agreement between the SIRU and EKF angles indicated good PAD performance.

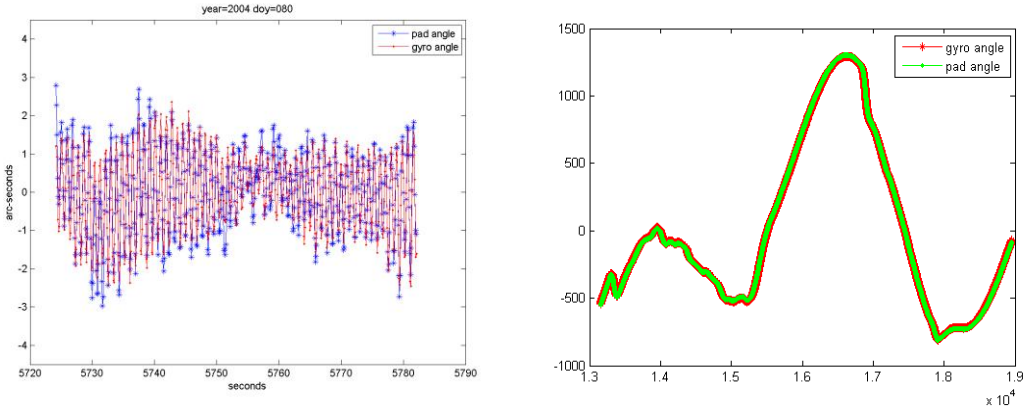


**(a) time interval: ~60 seconds** **(b) time interval: 5800 seconds (1 orbit revolution)**

**Figure 13. Comparison of the EKF angles to SIRU angles for longer time intervals than possible with LRS star. In the legend, PAD angle means angles derived from EKF quaternions.**

The difference of the two curves in Figure 13b is shown in Figure 14. The difference curve has characteristics similar to the CRS curve showing IST alignment motion in Figure 5b. The batch-EKF method created to replace the CRS exploits this similarity. The batch-EKF method differences SIRU attitudes and EKF attitudes. The difference of SIRU angles and EKF angles in Figure 14 contains very similar information.

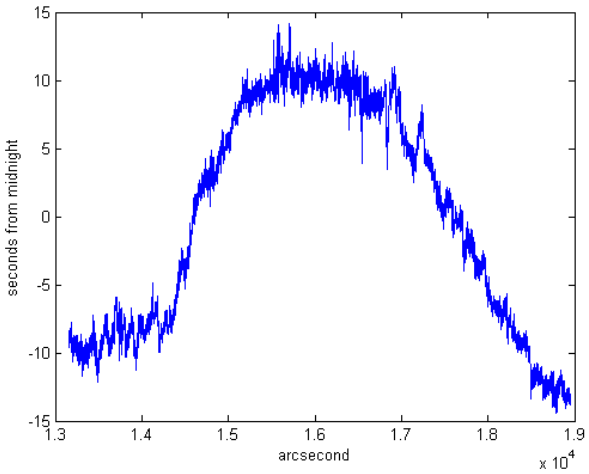


**Figure 14. Differences between EKF-derived angles and SIRU angles from Figure 13b**

## CONCLUSION

The LRS has proven flexible in resolving diverse issues: variations of the IST alignment, variations of the laser spot position, 0.1 second IST time-tag shifts, and a 50 millisecond gyro time-tag offset. Without the LRS these issues would have been difficult to detect or correct, and it would have been difficult to meet the pointing requirement. The LRS also provided independent validation of the attitude estimates thanks to its high resolution star measurements.

The LRS-2 for the ICESat-II mission is currently being designed for launch around 2015. The conceptual architecture is similar to the ICESat Stellar Reference System, but many functions will be combined into a single device. The LRS-2 will in effect combine into a single box what were the LRS, IST, and LPA. The major attitude and pointing instrument remaining outside the LRS will be an inertial reference unit.

## REFERENCES


[1] Zwally, J., et al., "ICESat's laser measurements of polar ice, atmosphere, ocean and land", *Journal of Geodynamics*, V. 34, 405-445, 2002.

[2] Abshire, J. B., et al, "Geoscience Laser Altimeter System (GLAS) on the ICESat mission: On-orbit measurement performance", *Geophys. Res. Letter*, 21, L21S02, doi:10.1029/2005GL024028, 2005.

[3] GLAS Instrument Team, Geoscience Laser Altimeter System science requirements, Version 2.01, October 1997.

[4] Bae. S., Schutz, B., and Sirota, M., "ICESat/GLAS laser pointing determination", *AAS/AIAA Spaceflight Mechanics Meeting*, Paper AAS 02-126, San Antonio, TX, January 2002.

[5] Luthcke, S., Rowlands. D., McCarthy. J., Pavlis., D., and Stoneking., E., "Spaceborne laser altimeter poining bias calibration from range residual analysis", *Journal of Spacecraft and Rockets*, Vol. 27, No. 3, 374-384, 2000.

[6] Magruder. L., Schutz. B., and Silverberg. E., "Laser pointing angle and time of measurement verification of the ICESat laser altimeter using a ground-based electro-optical detection system", *Journal of Geodesy*, Vol. 77, 148-153, 2003.

[7] Schutz. B., GLAS altimeter post-launch calibration and validation plan, Version 1.00, October 2000.

[8] Bae, S., Webb. C., and Schutz. B., "Star tracker misalignment calibration for the ICESat mission", *AAS/AIAA Spaceflight Mechanics Meeting*, Paper AAS 06-107, Tampa, FL, January 2006.

[9] Urban. T., and Schutz, B., "ICESat sea level comparisons", *Geophys. Res. Letter*, 32, L23S10, doi:10.1029/2005 GL024306, 2005.

[10] Bae, S., Ricklefs, R., Smith, N., and Schutz, B., "Time tag issues in the star tracker and gyro data for ICESat precision attitude determination", *AAS/AIAA Spaceflight Mechanics Meeting*, Paper AAS 09-128, Savannah, GA, February 2009.

[11] Shuster, M., and Oh, S., "Three-axis attitude determination from vector observations", *J. Guidance, Control, and Dynamics*, 4(1), 70-77, 1981.